Picosecond all-optical switching and dark pulse generation in a fibre-optic network using a plasmonic metamaterial absorber

Angelos Xomalis[1,2,*], Iosif Demirtzioglou[1], Yongmin Jung[1], Eric Plum[1,2,*], Cosimo Lacava[1], Periklis Petropoulos[1], David J. Richardson[1], and Nikolay I. Zheludev[1,2,3]

[1]*Optoelectronics Research Centre, University of Southampton, Highfield, Southampton, SO17 1BJ, UK*
[2]*Centre for Photonic Metamaterials, University of Southampton, Highfield, Southampton, SO17 1BJ, UK*
[3]*Centre for Disruptive Photonic Technologies, SPMS, TPI, Nanyang Technological University, Singapore 637371, Singapore*

[*]Email: ax1c15@soton.ac.uk, erp@orc.soton.ac.uk

Abstract

Coherent interaction of two light waves on a film of subwavelength thickness provides remarkable opportunities for controlling intensity and polarization of light beams as well as all-optical image processing. Here we show that such interactions can be used for optical dark pulse generation and basic all-optical signal processing in fully fiberized coherent information networks with 1 THz bandwidth. With an encapsulated plasmonic metamaterial absorber operating in the telecommunications C-band, we demonstrate switching and dark pulse generation with 1 ps laser pulses.

Nonlinear optics has given rise to all-optical signal processing by allowing optical signals to modulate one-another [1]. However, nonlinear methods require sufficient intensity to achieve a significant nonlinear response and face trade-offs between speed and magnitude of the nonlinearity involved [2-8]. In contrast, all-optical processing of mutually coherent signals does not require optical nonlinearity [9]. Similarly, nonlinear dark pulse generation [10-19] and nonlinear dark soliton propagation [10, 20-23] in optical fibres at high intensities are well-known, but the shortest dark pulses have been generated by linear methods in free space [21, 24]. Recent developments in dark pulse generation and coherent all-optical signal processing exploit the fact that modulation of light with light may be derived from the interaction of mutually coherent optical signals in a linear material of substantially subwavelength thickness [25]. Such all-optical modulation allows control over the absorption of light from "coherent perfect absorption" to "coherent perfect transmission" and is intensity-independent down to single photon signal levels [26]. It has enabled 11 fs dark pulse generation [24], polarization modulation, image processing and various logic functions in free space [25]. Recently, the concept was applied to demonstrate NOT, XOR and AND functions at up to 40 Gbit/s in a fibre-optic interferometer [27].

Standard single-mode optical fibres transmit 1 ps optical pulses in the C-band over several meters without any significant temporal broadening due to dispersive effects. This allows the realization of fibre networks that exploit coherent techniques for controlling light with light at high bandwidths. Here we demonstrate that coherent absorption and coherent transparency enable controlled absorption and transmission of mutually coherent 1 ps pulses in a fibre-optic network containing a pigtailed metadevice at wavelengths ranging from 1530 to 1560 nm. Our measurements imply a modulation bandwidth of at least 1 Tbit/s and indicate that the all-optical logic functions of ref. 27 may be performed at this rate (or even faster). Using 1 ps pulses to trigger coherent absorption of the central part of few ps pulses, we generate 1 ps dark pulses. Such linear in-fibre dark pulse generation is compatible with arbitrarily low intensities and may be used to convert arbitrary patterns of bright pulses into dark pulses.

The all-optical modulator is based on the linear interaction of light with light in a thin absorber. Two co-polarized, counter-propagating and mutually coherent input pulses in channels α and β interact in a lossy metasurface of deeply subwavelength thickness resulting in two output pulses in channels γ and δ. A standing wave forms as coherent input pulses of parallel linear polarization and equal intensity pass through each other. The metasurface is sufficiently thin to be placed at a node of the standing wave, where the electric field is zero due to destructive interference, or at an anti-node, where the electric field amplitude is enhanced by constructive interference. When it is located at a standing wave node, the light pulses cannot interact with the metasurface, rendering the structure perfectly transparent. In contrast, the pulses will interact strongly with the metasurface when it is placed at a standing wave anti-node, resulting in enhanced absorption. In the case of an ideal planar absorber this allows, in principle, the

absorption of the optical pulses to be modulated from 0% to 100% [25].

The lossy metasurface is the functional element within a fibre-optic metadevice with standard pigtailed FC/APC connectors which ensure compatibility with telecommunication fibre components (Fig. 1a). The metasurface was fabricated on the end face of a flat-cleaved single-mode polarization-maintaining optical fibre. A 70-nm-thick layer of gold was thermally evaporated onto the fibre's end face followed by focused ion beam milling of a 25 × 25 μm^2 array of asymmetrically split ring apertures through the gold layer covering the fibre core with the symmetry axis of the metasurface aligned to the slow axis of the Panda style fibre (Fig. 1b). The metamaterial-covered fibre was then coupled with a second cleaved optical fibre. To maximize the coupling efficiency and for ease of alignment, the fibre output was collimated and then focused onto the core of the second fibre using two anti-reflection-coated microcollimator lenses (Fig 1a). The components were fixed in place with glass and metal ferrules and bonded with UV-cured adhesive. The resulting assembly was placed in a protective stainless steel package.

We characterized the functionalities of a polarization-maintaining fibre interferometer containing the metadevice (Fig. 2). A fibre-coupled tunable continuous wave laser (Keysight 81940A) was launched into a frequency comb generator (OptoComb LP-5011), which produced 1 ps optical pulses at a repetition rate of 10 GHz. Then the pulsed signal was amplified and split into the two interferometer arms. One arm contained an optical delay line for adjusting the relative arrival times of pulses in channels α and β at the metasurface. The delay line was combined with a polarization controller and a polarization beam splitter that were used to monitor and minimize the unwanted orthogonal polarization component. The two arms were recombined within the metadevice and the output signals were detected via circulators using a fast sampling oscilloscope (EXFO PSO-102). Variable optical attenuators were used to prevent optical damage on the metasurface and to balance the peak power of the optical pulses in the two arms. In all experiments, the incident electric field was oriented parallel to the symmetry axis of the metasurface. While our fibre interferometer is stable on sub-second timescales, which is sufficient for proof-of-principle demonstrations, we note that practical applications would require active stabilisation of the optical path lengths to prevent phase drift in the interferometer.

The absorption of coherent optical pulses entering the metadevice depends on the phase difference between the input pulses at the position of the metasurface. It is instructive to consider the limiting cases, which are illustrated by Fig. 3 for equal-intensity input pulses of 1 ps duration, 1550 nm central wavelength, 10 GHz repetition rate and 0.4 mW average power in channels α and β (Fig. 3a). Destructive interference of these input pulses on the metasurface causes negligible light-metasurface interaction and thus little absorption, resulting in large output pulses in channels γ and δ (Fig. 3b, top). In contrast, constructive interference on the

metasurface enhances the light-metasurface interaction, causing strong absorption of the input pulses that results in suppression of the output pulses (Fig. 3b, bottom). Thus, the phenomena of coherent transmission and coherent absorption allow both 1 ps optical pulses to be either simultaneously transmitted or simultaneously absorbed in the metadevice.

Linear modulation of light with light is well-known in interferometers, where mutually coherent signals are usually combined by an essentially lossless beam splitter or fibre coupler. For comparison, we repeated the same experiment using a 50:50 fibre coupler (Fig. 3c) instead of the metadevice (Fig. 3b). Both the metadevice, which may be seen as approximating an ideal lossy beam splitter [28], and the 50:50 fibre coupler, which may be seen as approximating an ideal lossless beam splitter, allow modulation of the output pulses in channels γ and δ. However, the modulation mechanisms and the resulting relationships between the output signals are different. The coupler modulates light by redistributing power without losses in the ideal case, thus maximizing one coupler output will minimize the other (cases I and II in Fig. 3c). In contrast, the metadevice modulates light by controlling absorption, resulting in output signals that are simultaneously maximized or simultaneously minimized (Fig. 3b). Therefore, 4-port data processing devices based on coherent interactions on lossless and lossy beam splitters are fundamentally different and may be used in different applications and signal processing architectures.

To characterize the performance of the switching network we introduce the notion of modulation contrast, which is the ratio between peak powers in an output channel for the coherent transmission and absorption regimes. An ideal metadevice without coupling losses, that could provide infinite contrast for both outputs, would contain a metasurface that transmits and reflects 25% and absorbs 50% of any single input signal [25]. The asymmetric construction of our metadevice, that is based on a metasurface fabricated on the glass/air interface of a cleaved optical fibre, results in different optical properties for input signals in channels α and β (Fig. 4a). However, the asymmetry is small around the telecommunications C-band that covers the 1530 nm – 1565 nm wavelength range. For example, a single input signal of 1550 nm wavelength in channel α (β) will experience about 15% (15%) transmission, 22% (20%) reflection and 63% (65%) losses including coupling losses. These optical properties vary slowly with wavelength indicating that the metadevice can operate over a broad spectral range. Indeed, measurements of the peak power ratio of coherently transmitted pulses to coherently absorbed pulses yield a modulation contrast of 2 to 5 (3-7 dB) for both output channels, γ and δ, for the entire 1530 to 1560 nm wavelength range that is accessible by our experimental setup (Fig. 4b). Here, peak powers were determined by Gaussian fits (lines in Fig. 3) in order to exclude statistical noise affecting the data points.

Important opportunities for pulse shaping and dark pulse generation arise from combining mutually coherent signals of different shapes within the metadevice. We

introduced a tuneable bandwidth spectral filter for pulse broadening in one interferometer arm (Fig. 2) in order to study the interaction of 1 ps pulses with few ps pulses. The pulses in the input channels α and β had 1550 nm central wavelength, 10 GHz repetition rate and sub-mW average power. We recorded the metadevice's higher-contrast output channel δ, that had to be amplified for detection due to the reduced peak power imposed by pulse broadening (Fig. 5). The reflected 1 ps pulses from input channel α and the transmitted broadened pulses from input channel β were first separated in time, with the delay line, and detected at output channel δ (top row). In order to compensate for the metadevice's asymmetry, the detected pulse peak power of both pulses was matched by adjusting the variable optical attenuators in the interferometer arms. Then the pulses were overlapped in time. Depending on the mutual phase of the two input pulses, the 1 ps pulse may either suppress or increase the metasurface absorption in the region of temporal pulse overlap. Thus, in the case of coherent transparency we measured a bright 1 ps power burst at the center of the broadened pulse (middle row), while we measured a 1 ps trough in the signal in the case of coherent absorption (bottom row). Such rapid dips in power on a bright background are known as "dark pulses". We note that Erbium-Doped Fibre Amplifier (EDFA) amplification provides more gain to lower average power signals [i.e. the measurements in the middle (bottom) row of Fig. 5 are less (more) amplified than the reference measurements in the top row]. A comparison of the bright burst power (dark pulse power) with the power of the broader pulse, that is visible just before and after the bright burst (dark pulse), reveals a typical power change of 3× to 4× due to the presence of the second pulse. This indicates that the modulation contrast between bright bursts and dark pulses is about 10 dB in this experiment that compensates for the metadevice asymmetry.

Our results show that a fibre-optic network containing a plasmonic metamaterial absorber of nanoscale thickness allows controlled absorption and transmission of coherent optical signals with 1 ps time resolution, corresponding to a modulation bandwidth of 1 Tbit/s (in the telecommunications C-band). We have previously shown that coherent absorption and coherent transparency enable logic NOT, XOR and AND functions at up to 40 Gbit/s [27]. While we are not able to generate faster data signals, our results indicate that our fibre-optic interferometer with its metamaterial absorber could perform these functions at data rates as high as 1 Tbit/s. We expect that the fiberized system may have a modulation bandwidth of a few Tbit/s, which is limited by pulse broadening due to dispersion in the optical fibres rather than coherent absorption that occurs on a timescale of tens of femtoseconds [24]. Dispersion in the interferometer may be described by the average dispersion and differences of dispersion between the interferometer arms. The average dispersion changes the overall pulse width, could be exploited for compression of pre-chirped pulses and does not affect the achievable modulation contrast. Significant dispersion differences across the spectral pulse width (3.5 nm for 1 ps Gaussian pulses) would degrade the modulation contrast as different spectral components would interfere with different phase differences on the metasurface. However, such dispersion differences may be

avoided by carefully managing the dispersion introduced by the components included in the two arms of the interferometer.

By allowing bright pulses to trigger coherent absorption of a carrier signal, our fibre-optic network with metamaterial absorber can be used to convert an arbitrary sequence of bright pulses into dark pulses. Such an arbitrary dark pulse pattern generator without minimum intensity requirements could find uses in signal processing, dark soliton generation, nonlinear optics [29] and spectroscopy [30].

In summary, we have demonstrated all-optical control of optical signals with THz bandwidth in a fibre-optic network containing a plasmonic metamaterial absorber. Interaction of mutually coherent optical signals on a lossy metasurface enables controlled transmission and absorption of 1 ps optical pulses, as well as pulse shaping and 1 ps dark pulse generation. As the underlying mechanism of coherent perfect absorption and coherent perfect transmission is linear, such signal processing is possible at any level of intensity down to the quantum regime [26]. Potential applications include fast and energy-efficient all-optical information processing, coherent quantum information networks, pulse shaping and arbitrary dark pulse pattern generation at 1 Tbit/s.

This work is supported by the UK's Engineering and Physical Sciences Research Council (grants EP/M009122/1 and EP/P003990/1) and the MOE Singapore (grant MOE2016-T3-1-006).

Following a period of embargo, the data from this paper will be available from the University of Southampton ePrints research repository: http://doi.org/10.5258/SOTON/D0526

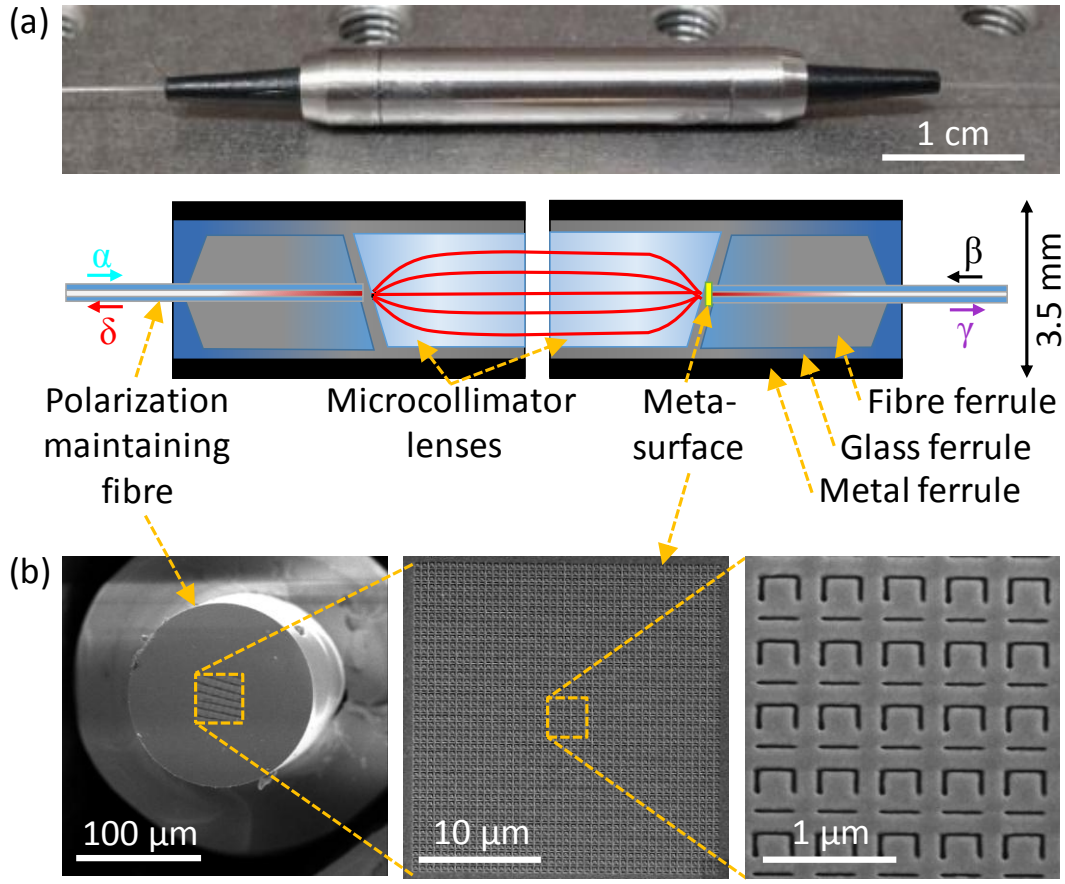

Figure 1: Fibre-optic metadevice for signal processing and dark pulse generation based on coherent absorption. (a) Photograph and schematic of the fibre-optic metadevice. Within the metadevice, coherent optical pulses in input channels α and β interact in a metasurface absorber, resulting in output pulses in channels γ and δ. (b) Scanning electron microscopy images of the metamaterial absorber that consists of a nanostructured gold film of 70 nm thickness and covers the core area of a single-mode polarization-maintaining optical fibre.

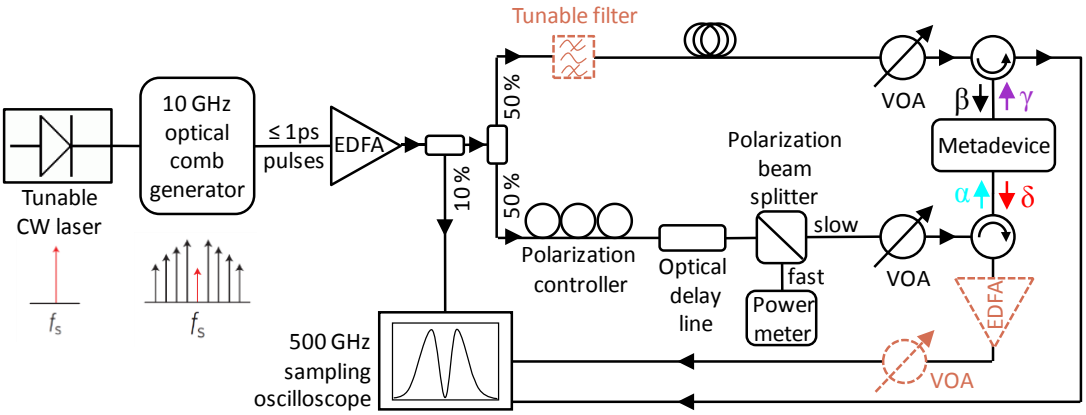

Figure 2: Coherent signal processing and dark pulse generation. Experimental setup for controlled absorption and transmission of 1 ps pulses (black lines) with additional components required for dark pulse generation and detection (brown dashed lines). VOA - Variable Optical Attenuator, EDFA - Erbium Doped Fibre Amplifier.

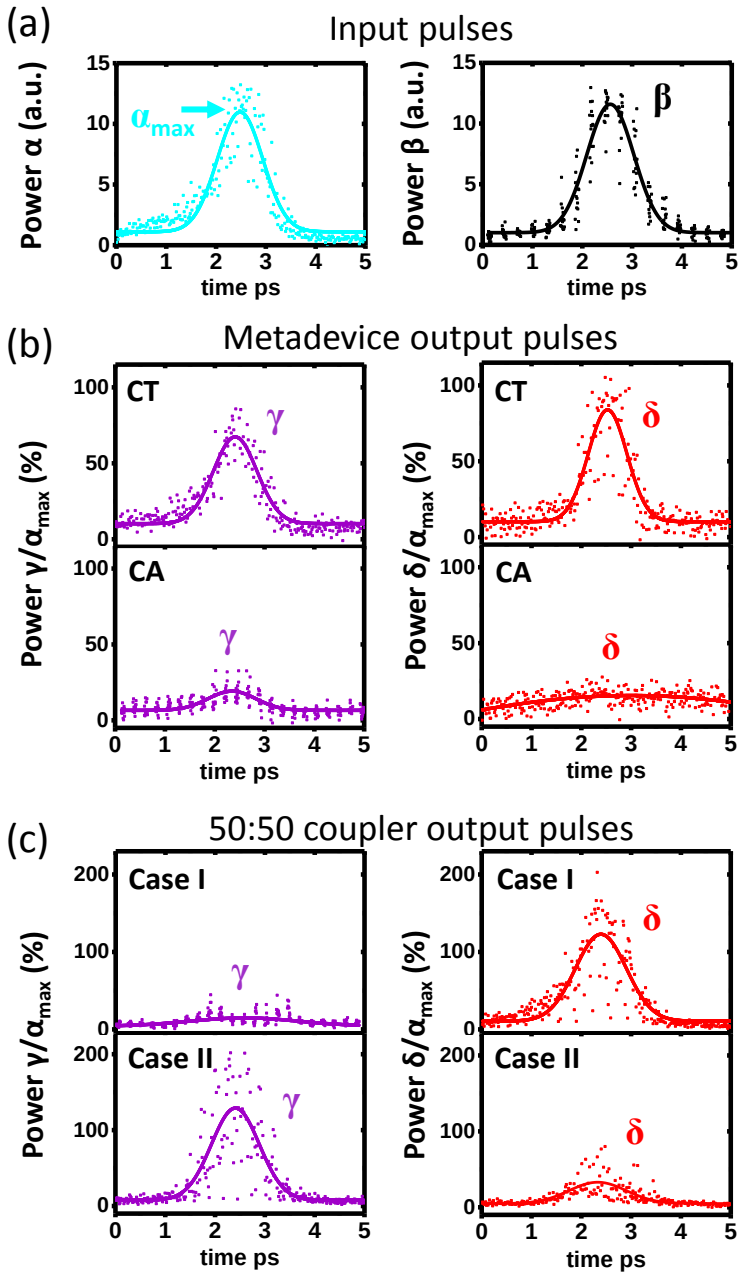

Figure 3: Controlled absorption and transmission of 1 ps pulses. (a) Power profiles of the coherent input pulses in channels α and β. (b) Power profiles of the output pulses in channels γ and δ in the cases of destructive (top) and constructive (bottom) interference on the metasurface absorber. These cases correspond to Coherent Transmission (CT) and Coherent Absorption (CA), respectively. (c) Power profiles of the output pulses in channels γ and δ measured after replacing the metadevice with a low-loss 50:50 fibre coupler in case of constructive interference of the input pulses in output channel δ (Case I) or γ (Case II). For clarity, all pulses are presented with Gaussian fits (lines).

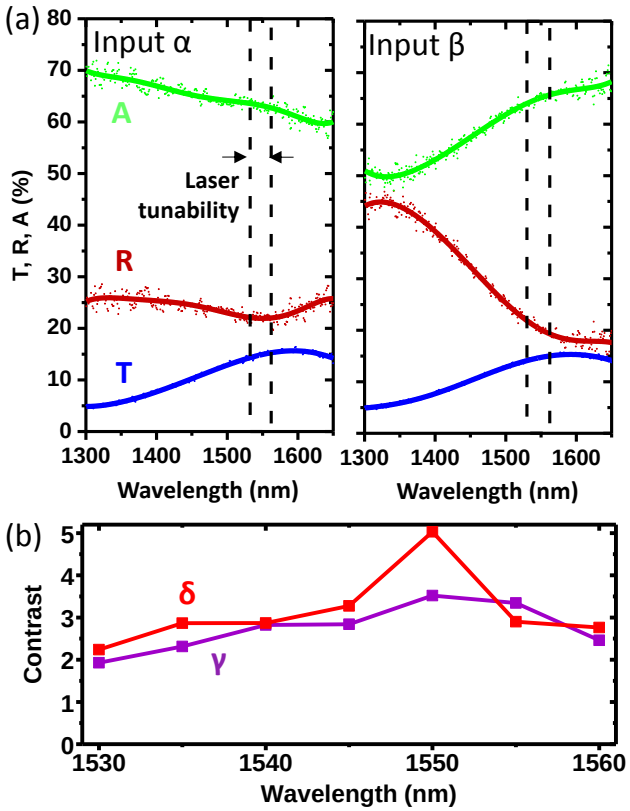

Figure 4: Broadband signal processing. (a) Metadevice transmission (T), reflection (R) and absorption (A) as measured with light entering the metadevice from either input α (left) or β (right). The data points are shown with polynomial fits (lines). (b) Modulation contrast observed for output channels γ and δ as functions of laser wavelength.

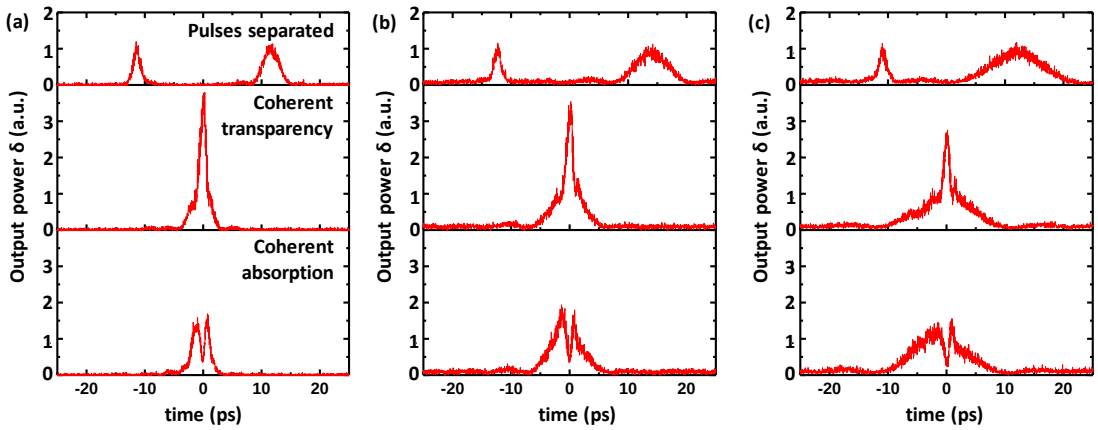

Figure 5: Generation of 1 ps dark pulses. Output power in channel δ in the cases when the input pulses in channels α and β are separated in time (top); the pulses overlap in the coherent transparency regime (middle); the pulses overlap in the coherent absorption regime (bottom). The columns correspond to different durations of the input pulses in channel β of (a) 3 ps, (b) 6 ps and (c) 9 ps. In all cases, the duration of the pulses in channel α was 1 ps.

References:

1. P. Singh, D. K. Tripathi, S. Jaiswal, and H. K. Dixit, Advances in Optical Technologies **2014**, 275083 (2014).
2. R. W. Boyd, *Nonlinear Optics*, 3rd ed. (Academic Press, 2008) p. 211.
3. D. Cotter, R. J. Manning, K. J. Blow, A. D. Ellis, A. E. Kelly, D. Nesset, I. D. Phillips, A. J. Poustie, and D. C. Rogers, *Science* **286**, 1523 (1999).
4. V. R. Almeida, C. A. Barrios, R. R. Panepucci, and M. Lipson, *Nature* **431**, 1081 (2004).
5. Q. Xu and M. Lipson, *Opt. Express* **15**, 924 (2007).
6. K. Nozaki, T. Tanabe, A. Shinya, S. Matsuo, T. Sato, H. Taniyama, and M. Notomi, *Nature Photonics* **4**, 477 (2010).
7. A. E. Willner, S. Khaleghi, M. R. Chitgarha, and O. F. Yilmaz, *J. Lightwave Technol.* **32**, 660 (2014).
8. C. Lacava, M. A. Ettabib, and P. Petropoulos, *Appl. Sci.* **7**, 103 (2017).
9. X. Fang, K. F. MacDonald, and N. I. Zheludev, *Light. Sci. Appl.* **4**, e292 (2015).
10. D. Krökel, N. J. Halas, G. Giuliani, and D. Grischkowsky, *Phys. Rev. Lett.* **60**, 29 (1988).
11. D. Meshulach and Y. Silberberg, *Nature* **396**, 239 (1998).
12. J. Zimmermann, *Appl. Phys. Lett.* **79**, 18 (2001).
13. H. Zhang, D. Y. Tang, L. M. Zhao, and X. Wu, *Phys. Rev. A* **80**, 045803 (2009).
14. M.Feng, K. L. Silverman, R. P. Mirin, and S. T. Cundiff, *Opt. Express* **18**, 13385 (2010).
15. X. Li, S. Zhang, Y. Meng, and Y. Hao, *Opt. Express* **21**, 8409 (2013).
16. H. H. Liu and K. K. Chow, *Opt. Express* **22**, 29708 (2014).
17. W. Liu, L. Pang, H. Han, W. Tian, H. Chen, M. Lei, P. Yan, and Z. Wei, *Opt. Express* **23**, 26023 (2015).
18. X. Xue, Y. Xuan, Y. Liu, P.-H. Wang, S. Chen, J. Wang, D. E. Leaird, M. Qi, and A. M. Weiner, *Nat. Photonics* **9**, 594 (2015).
19. J. Liu, X. Li, S. Zhang, H. Zhang, P. Yan, M. Han, Z. Pang, and Z. Yang, *Sci. Rep.* **6**, 29128 (2016).
20. A. Hasegawa and F. Tappert, *Appl. Phys. Lett.* **23**, 171 (1973).
21. A. M. Weiner, J. P. Heritage, R. J. Hawkins, R. N. Thurston, E. M. Kirschner, D. E. Leaird, and W. J. Tomlinson, *Phys. Rev. Lett.* **61**, 2445 (1988).
22. A. M. Weiner, R. N. Thurston, W. J. Tomlinson, J. P. Heritage, D. E. Leaird, E. M. Kirschner, and R. J. Hawkins, *Opt. Lett.* **14**, 868 (1989).
23. W. Zhao and E. Bourkoff, *Opt. Lett.* **14**, 703 (1989).
24. V. Nalla, J. Valente, H. Sun, and N. I. Zheludev, *Opt. Express* **25**, 22620 (2017).
25. E. Plum, K. F. MacDonald, X. Fang, D. Faccio, and N. I. Zheludev, *ACS Photonics* **4**, 3000 (2017).
26. T. Roger, S. Vezzoli, E. Bolduc, J. Valente, J. J. F. Heitz, J. Jeffers, C. Soci, J. Leach, C. Couteau, N. I. Zheludev, and D. Faccio, *Nat. Commun.* **6**, 7031

(2015).
27. A. Xomalis, I. Demirtzioglou, E. Plum, Y. Jung, V. Nalla, C. Lacava, K. F. MacDonald, P. Petropoulos, D. J. Richardson, and N. I. Zheludev, *Nat. Commun.* **9**, 182 (2018).
28. S. Thongrattanasiri, F. H. L. Koppens, and F. J. García de Abajo, *Phys. Rev. Lett.* **108**, 047401 (2012).
29. Y. S. Kivshar and B. Luther-Davies, *Phys. Rep.* **298**, 81 (1998).
30. R. W. Schoenlein, S. Chattopadhyay, H. H. W. Chong, T. E. Glover, P. A. Heimann, C. V. Shank, A. A. Zholents, and M. S. Zolotorev, *Science* **287**, 2237 (2000).